Optical Materials 36 (2013) 425–436

Contents lists available at ScienceDirect

Optical Materials

journal homepage: www.elsevier.com/locate/optmat

Effects of molarity and solvents on the optical properties of the *solutions* of tris[4-(5-dicyanomethylidenemethyl-2-thienyl)phenyl]amine (TDCV-TPA) and structural properties of its film

Bayram Gündüz *

Department of Science Education, Faculty of Education, Muş Alparslan University, Muş 49250, Turkey

ARTICLE INFO

Article history:
Received 7 August 2013
Received in revised form 2 October 2013
Accepted 3 October 2013
Available online 25 October 2013

Keywords:
TDCV-TPA
Surface roughness parameters
Molar/mass extinction coefficient
Molarity
Optical band gap
Optical parameters

ABSTRACT

The surface morphology of the tris[4-(5-dicyanomethylidenemethyl-2-thienyl)phenyl]amine (TDCV-TPA) film was investigated by high performance atomic force microscopy and the surface roughness parameters such as roughness average (*sa*), root mean square roughness (*sq*), surface skewness (*ssk*) and surface kurtosis (*sku*) of the TDCV-TPA film were obtained. The TDCV-TPA film indicated the low valleys with bumpy surface. The optical properties of the *solutions* of the small-molecule semiconducting dye TDCV-TPA for different high molarities, lower molarities and different solvents were investigated in detail. The molar extinction coefficient, optical band gap, angle values of refraction of the TDCV-TPA decreased with increasing molarity, while the absorbance at maximum absorption wavelengths, angle of incidence, electric susceptibility, real part values of the optical conductivity of the TDCV-TPA increased with increasing molarity. The maximum molar extinction coefficient (ε_{max}) at λ_{max} values (510 and 509 nm) of the solutions of the TDCV-TPA for 0.024 and 0.010 mM were found to be 1.175×10^5 and 1.931×10^5 L mol^{-1} cm^{-1}, respectively. The maximum mass extinction coefficient (α_{max}) of the solutions of the TDCV-TPA for 0.024 and 0.010 mM were found to be 163.226 and 268.247 L g^{-1} cm^{-1}, respectively. The optical band gap (E_g) values of the TDCV-TPA for 1, 2 and 3 mM were found to be 1.916, 1.898 and 1.892 eV, respectively. The absorption band edge for DCM varied from 1.882 to 1.997 eV, while the absorption band edge for chloroform varied from 1.923 to 2.027 eV. To obtain lower optical band gap of the TDCV-TPA can be prefered DCM solvent.

1. Introduction

Organic semiconductors (OSCs) have been studied since the early 1950s [1], dealing essentially with small molecules, e.g., condensed hydrocarbons and dyes. OSCs are generally divided in two groups such as low molecular weight semiconductors based on small organic molecules and polymers with higher molecular weight [2,3]. OSCs such as linear π-conjugated systems [4] are the focus of growing scientific and technological interest, motivated by their potential application in flexible and cost-effective opto-electronic devices, for example, field effect transistors (FETs) [5–9] light-emitting diodes (LEDs) [10–12] and solar cells [13–16]. These devices require active materials able to perform a specific function, such as charge transport, light-emission, or light harvesting [5]. Small molecules are light and can usually be purified and deposited through thermal evaporation processes [17]. In recent years, organic materials have received increased interest for their easy process, flexibility [18], low-cost manufacturing, easy processing and interesting sensing properties or high luminescence efficiencies [19] and for many components of electronic devices, particularly the active semiconductor layer, due to many fundamental advantages as the active material in optical and electronic devices [20], such as chemical sensors [21,22], light emitting diodes, solar cells [20], smart cards, electronic displays, radio frequency identification tags [23], thin film transistors [24] and field-effect transistors [20] over their inorganic counterparts [25]. This large range of possible applications can be realized by understanding the basic science in involved in the operation of organic electronic devices and the physics of organic semiconductors [2]. The application of organic electronics can range from polymer micro-electronic mechanical-systems to organic superconductors [26]. Triarylamines substituted by acceptor groups are promising as deep-red-light emitters for doped and nondoped organic LED devices [5]. Triphenylamine (TPA) derivatives are well-known for their star-shape dendrimer structure [27], their 3D propeller shape and glass-forming properties and are widely used as 3D conjugated systems of organic semiconductors with hole-injecting/transporting behavior or luminophore materials in LEDs [5,28,29]. It is known that TPA-based compounds have been widely applied as

* Tel.: +90 4362130013 2104; fax: +90 4362120853.
E-mail addresses: bgunduz83@hotmail.com, b.gunduz@alparslan.edu.tr

0925-3467/$ - see front matter © 2013 Elsevier B.V. All rights reserved.
http://dx.doi.org/10.1016/j.optmat.2013.10.005

hole transport and electroluminescence materials [28,30–34], and their amorphous character offers the possibilities to develop active materials for the fabrication of organic solar cells with isotropic optical and charge transport properties [30]. Thienylenevinylene-triphenylamine functionalized with peripheral dicyanovinylene groups (TDCV-TPA) was designed as an isotropic material for solar cells [5]. TDCV-TPA displays an appreciable photoluminescence (PL) quantum efficiency [35]. The electroluminescence (EL) is in the deep-red region of the UV–vis spectrum, with an onset at 580 nm and a maximum at 658 nm [5].

Atomic Force Microscopy (AFM) image is significant in order to investigate structural properties of a material. AFM has become a popular method of investigating the surface structures of the materials and gives the surface topography images in one dimensional (1D)/three dimensional (3D) by scanning with a cantilever tip over a surface. The knowledge of the surface topography at nanometric resolution made possible to probe dynamic biological process [36,37], tribological properties [38,39], mechanical manufacturing [40] and mainly thin film surfaces [41,42]. It is a useful method to study morphology and texture of diverse surfaces of the materials because of the effect on the electrical and optical properties of the materials/devices [43].

The nonlinear optical properties, such as optical absorption [44,45], have shown high potential [46] for device applications in far- infrared laser amplifiers [47], photo-detectors [48], and high speed electro-optical modulators [49].

The extinction coefficients, including mass extinction coefficient (α) and molar extinction coefficient (ε), are parameters to define the absorbance intensity at a given wavelength per mass density (g) or molar concentration (mol), respectively [50–52]. It can be determined by using the Beer–Lambert law, $Abs = \varepsilon cl$, where *Abs* is the absorbance which can be obtained using a UV–vis absorbance spectrometer, and l is the optical path length [50,53]. An accurate molar concentration (c) needs to be determined to obtain the molar extinction coefficient (ε) [50].

Solvent affects on organic reactivity and on absorption spectra have been studied for more than a century [54]. It is well known that the photo-physical behavior of a dissolved dye depends on the nature of its environment [54], that is, the shape, intensity, and maximum absorption wavelength of the absorption band of dye in solution depends strongly on the solvent–solute interactions and solvent nature [54–58]. This effect is closely related to the nature and degree of dye–solvent interactions [54].

Solvents are effective on the optical and electrical properties of the materials. Dichloromethane (DCM), or methylene chloride, is an organic compound with the formula CH_2Cl_2. It is colorless, volatile liquid with a moderately sweet aroma and is widely used as a solvent. Although it is not miscible with water, it is miscible with many organic solvents [59]. DCM's volatility and ability to dissolve a wide range of organic compounds makes it a useful solvent for many chemical processes. Chloroform is an organic compound with formula $CHCl_3$. It is one of the four chloromethanes [59]. The colorless, sweet-smelling, dense liquid is a trihalomethane, and is considered somewhat hazardous [59]. Chloroform is a common solvent in the laboratory, because it is relatively unreactive, miscible with most organic liquids, and conveniently volatile [60]. Chloroform is an effective solvent for alkaloids in their base form and thus plant material is commonly extracted with chloroform for pharmaceutical processing.

Furthermore, some scientists made several researches on the surface morphology of the TDCV-TPA film. Bernede and co-workers [61] reported that the AFM images in three dimensions and profiles of TDCV-TPA films deposited onto ITO/MoO_3, and ITO/CuI structures, and two dimensions AFM images and profiles of TDCV-TPA films deposited onto ITO/MoO_3 and ITO/CuI structures. They [61] reported that the films present very different roughnesses with rms of 2.20 and 1.26 nm for MoO_3 and CuI, respectively. On the other hand, there is not any report in the literature about the surface roughness parameters such as roughness average (*sa*), root mean square roughness (*sq*), surface skewness (*ssk*) and surface kurtosis (*sku*) of the only TDCV-TPA film.

Some scientists made researches on some optical parameters of the TDCV-TPA film. Sulaiman and Fakir [27] reported that the spectrum of the TDCVTPA film extended into part of the UV region (200–400 nm) and covered the whole range of the visible region (400–700 nm). They [27] estimated the optical energy gap of the TDCV-TPA film as a 1.9 eV. Some scientists made many researches on the molar extinction coefficient and mass extinction coefficient of the some materials [50,62,63]. On the other hand, there is not any report in the literature about the optical properties of the *solutions* of the small-molecule semiconducting dye TDCV-TPA for different high molarities, lower molarities and different solvents. This solution technique for investigation of the optical properties of the soluble materials is cheaper than a film technique, because there is not need to any deposition devices such as spin-coater, Langmuir–Blodgett (LB) devices, which are more expensive devices to investigate the optical properties of the TDCV-TPA material. This solution technique is more accurate than a film technique, because prior, during and after the coating of a film, various impurities may occur on the surface of the film and these disadvantages adversely affect the optical properties of the material.

In this study, we investigated the surface morphology of the tris[4-(5-dicyanomethylidenemethyl-2-thienyl)phenyl]amine (TDCV-TPA) film by high performance atomic force microscopy and the surface roughness parameters such as roughness average (*sa*), root mean square roughness (*sq*), surface skewness (*ssk*) and surface kurtosis (*sku*) of the TDCV-TPA film were obtained. Then, we investigated in detail the optical properties of the *solutions* of the small-molecule semiconducting dye TDCV-TPA for different high molarities, lower molarities and different solvents. To examine optical properties, the TDCV-TPA material for different high molarities, lower molarities and different solvents homogeneously dissolved. The optical measurements were conducted on a Shimadzu model UV-1800 Spectrophotometer. The effects of the high molarities, lower molarities and solvents on the optical parameters such as molar extinction coefficient, mass extinction coefficient, average transmittance, absorb wavelength, absorption band edge, optical band gap, real and imaginary part of the dielectric constant, electrical susceptibility, real and imaginary part of conductivity were investigated.

2. Experimental

Tris[4-(5-dicyanomethylidenemethyl-2-thienyl)phenyl]amine (TDCV-TPA) small-molecule semiconducting dye and solvents, which are dichloromethane (DCM) and chloroform used in this study, were purchased from Sigma–Aldrich Co. The chemical structure of the TDCV-TPA small-molecule semiconducting dye is shown in Fig. 1. This section has been occurred in three stages. In the first stage, we prepared the TDCV-TPA film at high molarity for AFM image. In the second stage, we prepared the stock solutions of the TDCV-TPA for different high molarities, lower molarities and different solvents. In the last stage, we recorded the optical measurements of the stock solutions of the TDCV-TPA for different high molarities, lower molarities and different solvents.

2.1. Preparation of the TDCV-TPA film at high molarity for AFM image

To prepare the TDCV-TPA film, the TDCV-TPA material weighed with a AND-GR-200 Series Analytical Balance for 3 mM, then it was dissolved homogeneously in 4 mL volume of DCM and it was

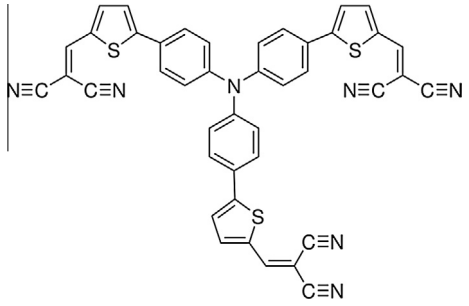

Fig. 1. The chemical structure of the TDCV-TPA small-molecule semiconducting dye.

filtered through PTFE membrane filter to obtain the best film. Ultimately, the filtered solution of the TDCV-TPA was deposited on cleaned microscopy glass at 2000 rpm for 20 s by the spin coating method. After the spin coating, the film was dried at 70 °C for 5 min to evaporate the solvent and remove organic residuals. Surface morphology of the TDCV-TPA film was investigated by high performance atomic force microscopy (hpAFM, NanoMagnetics Instruments Co.) with PPP-XYNCHR type Cantilever at dynamic mode.

2.2. Preparation of the stock solutions of the TDCV-TPA for different high molarities, lower molarities and different solvents

The molecular weight and formula of the TDCV-TPA small-molecule semiconducting dye is 719.86 g/mol and $C_{42}H_{21}N_7S_3$, respectively. To prepare the stock solutions, firstly the TDCV-TPA material weighed with a AND-GR-200 Series Analytical Balance for 1, 2 and 3 mM of the high molarities, for 0.33, 0.12, 0.05, 0.024 and 0.010 mM of the lower molarities and for 2, 0.28 and 0.12 mM of the different solvents (DCM and chloroform). Then, these weighed TDCV-TPA materials dissolved homogeneously in 6 mL volume of DCM solvent for 1, 2 and 3 mM and in 4 mL volume of DCM solvent for 0.33, 0.12, 0.05, 0.024 and 0.010 mM, and in 4 mL volume of chloroform solvent for 2, 0.28 and 0.12 mM. Ultimately, prepared all the solutions of the TDCV-TPA were filtered through PTFE membrane filter to obtain the best results of the optical measurements. The real pictures of the filtered solutions of the TDCV-TPA for 2 mM dissolved in DCM and chloroform are shown in Fig. 2a and b, respectively.

2.3. The optical measurements of the stock solutions of the TDCV-TPA for different high molarities, lower molarities and different solvents

We used the cylindrical cuvettes (Hellma QS-100) of 3.5 mL volume and 10 mm optical path length for all the solutions of the TDCV-TPA. The optical measurements of all the solutions of the TDCV-TPA for different high molarities, lower molarities and different solvents were recorded by a Shimadzu model UV-1800 Spectrophotometer in the wavelength 1100–190 nm at room temperature.

3. Results and discussion

This section has been occurred in four stages. In the first stage, we investigated the surface morphology properties of the TDCV-TPA film. In the second stage, we investigated in detail the optical properties of the *solutions* of the TDCV-TPA for 1, 2 and 3 mM of the high molarities. The effects of the high molarity on the optical parameters such as molar extinction coefficient, average transmittance, absorption band edge, optical band gap were investigated. In

Fig. 2. The real pictures of the filtered solutions of the TDCV-TPA for 2 mM dissolved in (a) DCM and (b) chloroform solvent.

the third stage, we investigated in detail the optical properties of the *solutions* of the TDCV-TPA for 0.33, 0.12, 0.05, 0.024 and 0.010 mM of the lower molarities. The effects of the lower molarities on the optical parameters such as molar extinction coefficient, maximum mass extinction coefficient, average transmittance, absorb wavelength, absorption band edge, optical band gap, real and imaginary part of the dielectric constant, electrical susceptibility, real and imaginary part of conductivity were investigated. In the last stages, we investigated in detail the optical properties of the *solutions* of the TDCV-TPA for 2, 0.28 and 0.12 mM of the different solvents (DCM and chloroform). The effects of the DCM and chloroform solvents on the optical parameters such as molar extinction coefficient, average transmittance, absorb wavelength, absorption band edge, optical band gap were investigated.

3.1. Surface morphology properties of the TDCV-TPA film

Surface morphology properties of the TDCV-TPA film were investigated by high performance atomic force microscopy. The scan area was chosen as $5 \times 5\ \mu m^2$. Fig. 3a and b shows one (1D) and three dimensional (3D) AFM images of the TDCV-TPA film for $5 \times 5\ \mu m^2$ scan area, respectively. As seen in Fig. 3a and b, these images also have the light, dark and valley regions (pits). The color intensity as seen in Fig. 3a and b shows the vertical profile of the material surface, with light regions being the highest points and the dark points representing the depressions and pores [43].

The differences in the surface morphology of the TDCV-TPA film were investigated in terms of four types of roughness parameters

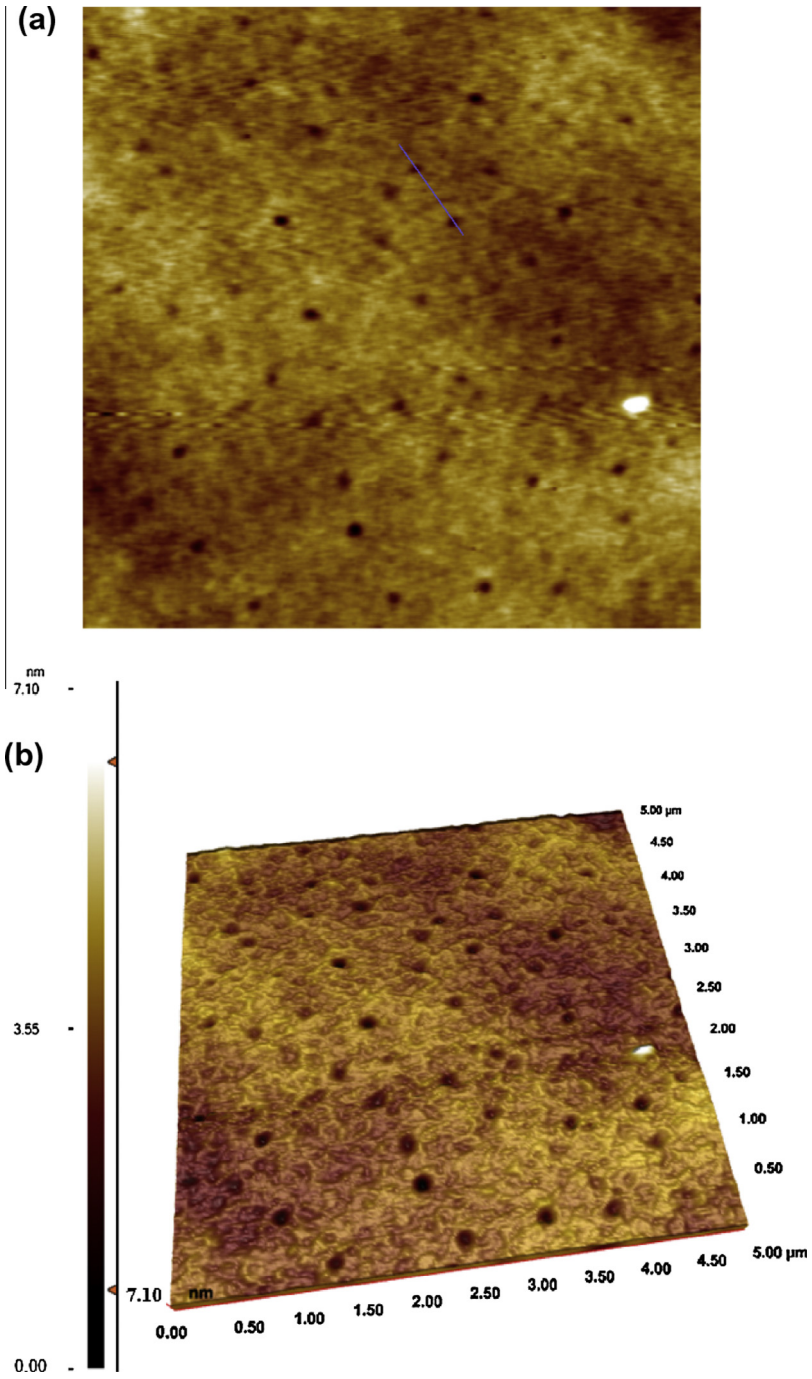

Fig. 3. (a) One (1D) and (b) three dimensional (3D) AFM images of the TDCV-TPA film.

such as; roughness average (*sa*), root mean square roughness (*sq*), surface skewness (*ssk*), and surface kurtosis (*sku*).

Roughness is known to inhibit the growth of uniform [64] and it is useful for detecting general variations in overall profile height characteristics and for monitoring an established manufacturing process [37].

Root mean square (RMS) roughness (*sq*) is the square root of the distribution of surface height and is considered to be more sensitive than the average roughness for large deviations from the mean line/plane and is also used in computing the skew and kurtosis parameters [37]. RMS roughness (*sq*) describes the finish of optical surfaces and represents the standard deviation of the profile heights and is used in computations of skew and kurtosis [37].

Surface roughness skewness (*ssk*) is used to measure the symmetry of the variations of a profile/surface about the mean line/plane and is more sensitive to occasional deep valleys or high peaks [37]. The negative values of the skewness indicate that the valleys are dominant over the scanned area and positive values show that the peaks are dominant on the surface [37]. Continued negative values would indicate cracks, representative of valleys [37]. The distribution of positive and negative values indicates the existence of protruding grains [37].

Kurtosis is a measure of the distribution of spikes above and below the mean line. Kurtosis describes machined surfaces and is rarely used for optical surfaces. It is sometimes specified for the control of stress fracture. Surface roughness kurtosis (*sku*) is used to measure the distribution of the spikes above and below the mean line/plane [37]. For the Gaussian distribution, the skewness is equal to zero and the kurtosis is equal to three [43].

In this study, the surface roughness parameters such as roughness average (*sa*), root mean square roughness (*sq*), surface skewness (*ssk*) and surface kurtosis (*sku*) of the TDCV-TPA film were obtained from the AFM images with an AFM software program.

The roughness average (0.352 nm) of the TDCV-TPA film is lower than that of the root mean square roughness (0.446 nm). The root mean square roughness (0.446 nm) of the TDCV-TPA film is smaller than that of the roughnesses (2.20 and 1.26, respectively) of the TDCV-TPA films on the MoO_3 and CuI in the literature [61]. For a Gaussian distribution of asperity height, statistical theory shows that the ratio of *sq* to *sa* should be 1.25. Ward [65] notes that the asperity height distribution of most engineering surfaces (tribology) may be approximated by a Gaussian distribution with *sq*/*sa* values of up to 1.31. The ratio (1.267) of *sq* to *sa* of the TDCV-TPA film is reasonably close to the value of 1.25 predicted by theory.

The surface skewness (−0.194) of the TDCV-TPA film is negative, which indicates the porous structure as seen also in Fig. 3a and b. The negative skew of the TDCV-TPA film attributes to a criterion for a good bearing surface and negative value of the skewness of the TDCV-TPA film indicates that the valleys are dominant over the scanned area [37]. Surfaces with a positive skewness, such as turned surfaces have fairly high spikes that protrude above a flatter average [43]. Surfaces with negative skewness, such as porous surfaces have fairly deep valleys in a smoother plateau [43]. More random (for example, ground) surfaces have a skewness of about zero [43]. A value of *ssk* greater than about 1.5 in magnitude (positive or negative) indicates that the surface does not have a simple shape and more advanced parameters are needed to fully describe the surface structure [43,66]. So, the surface of the TDCV-TPA film have a simple shape and more advanced parameters are needed to fully describe the surface structure because of the *ssk* ($|-0.194| < 1.5$ [43,66].

The surface kurtosis (4.633) of the TDCV-TPA film is higher than 3 which indicate the low valleys with bumpy surface as seen also in Fig. 3a and b. In the literature [37], for spiky surfaces, *sku* > 3; for bumpy surfaces, *sku* < 3; perfectly random surfaces have kurtosis 3. As seen in blue line region of the Fig. 3a, there are two pits. The first and second pits of the TDCV-TPA film are 1.89 and 1.29 nm deep, respectively. These deeps of the pits of the TDCV-TPA are considered as very important parameter due to giving a good description of the overall roughness of the surface [37].

3.2. The optical properties of the solutions of the TDCV-TPA for high molarities

The absorbance spectras of the solutions of the TDCV-TPA were taken to investigate their optical properties for 1, 2 and 3 mM of the high molarities. The molar extinction coefficient (ε) values of the solutions of the TDCV-TPA can be determined with an equation known as the Beer–Lambert law [53].

$$\varepsilon = \frac{Abs}{cl} \tag{1}$$

where *Abs* is an actual absorption, *l* is an optical path length, and *c* is the molar concentration of the used cuvettes. The ε values of the solutions of the TDCV-TPA material were calculated from Eq. (1). The molar extinction coefficient of the TDCV-TPA decreases with increasing molarity. It is observed that the molar extinction coefficient of the TDCV-TPA is the lowest for emitted red light at about 658 nm.

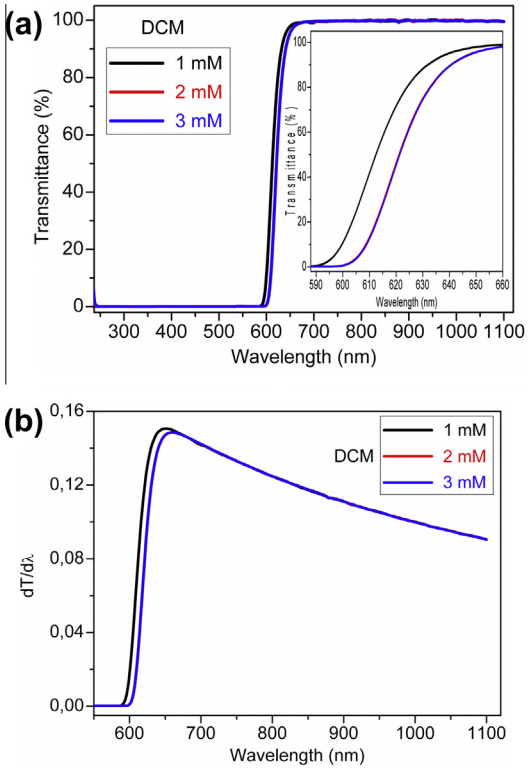

Fig. 4. (a) The plot of the transmittance vs. λ and (b) the curves of $dT/d\lambda$ vs. λ of the solutions of the TDCV-TPA for 1, 2 and 3 mM.

The transmittance spectras of the solutions of the TDCV-TPA were taken to investigate their optical properties for 1, 2 and 3 mM and the plot of the transmittance vs. wavelength is shown in Fig. 4a. As seen in Fig. 4a and its inset, the transmittance spectra of the solutions of the TDCV-TPA until about 580 nm are not observed due to the high molarity of the solutions of the TDCV-TPA, but the transmittance spectra of the solutions of the TDCV-TPA sharply increases in the range of about 580 and 658 nm. After about 658 nm, the transmittance spectras of the solutions of the TDCV-TPA are not again observed due to emitted red light at about 658 nm of the TDCV-TPA. In the visible region, the average transmittance (T_{avg}) values of the solutions of the TDCV-TPA were calculated and given in Table 1. As seen in Table 1, the T_{avg} (41.292%) for 1 mM is the highest, while the T_{avg} (39.098%) for 3 mM is the lowest. It is observed that the average transmittance values of the solutions of the TDCV-TPA in the visible region decrease with increasing molarity. To estimate the absorption band edge of the solutions of the TDCV-TPA, the first derivative of the optical transmittance can be computed. For this purpose, we plotted the curves of $dT/d\lambda$ vs. wavelength of the solutions of the TDCV-TPA for 1, 2 and 3 mM, as shown in Fig. 4b. The absorption band edge values of the solutions of the TDCV-TPA were calculated from the maximum peak position and given in Table 1. As seen in Table 1, the maximum peak values of the solutions of the TDCV-TPA vary from 652 to 659 nm. This result suggests that the absorption band edge of the solutions of the TDCV-TPA shifts from 1.902 to 1.882 eV with the increasing molarity.

The optical band gap (E_g) of optical transitions can be evaluated from the absorption spectrum using the Tauc relation [67–72]

$$(\alpha h\upsilon) = A(h\nu - E_g)^m \tag{2}$$

Table 1
The T_{avg} (in the visible region), $\lambda_{max.peak}$, absorption band edge, E_g values of the solutions of the TDCV-TPA for 1, 2 and 3 mM.

Molarity (mM)	T_{avg} (%)	$\lambda_{max.peak}$ (nm)	Absorption band edge (eV)	E_g (eV)
1	41.292	652	1.902	1.916
2	39.164	659	1.882	1.898
3	39.098	659	1.882	1.892

where A is a constant, $h\nu$ is the photon energy, E_g is the optical band gap of the material and m is the parameter measuring type of band gaps. For $m = 2$, E_g in Eq. (2) is indirect allowed band gap. To determine the optical band gap of the solutions of the TDCV-TPA for 1, 2 and 3 mM, the $(\alpha h\nu)^{1/2}$ plot vs. the photon energy E of the TDCV-TPA is shown in Fig. 5. As seen in Fig. 5, there is a linear region for the optical band gap E_g values of the TDCV-TPA. By extrapolating the linear plot to $(\alpha h\nu)^{1/2} = 0$, the E_g values of the TDCV-TPA were obtained and given in Table 1. As seen in Table 1, the E_g values of the TDCV-TPA decrease also with increasing molarity. The E_g value (1.916 eV) of the TDCV-TPA for 1 mM is the highest value of all the solutions, while the E_g value (1.892 eV) of the TDCV-TPA for 3 mM is the lowest value. The E_g values of the TDCV-TPA film were in agreement with the value (1.9 eV) in the literature [27]. This result suggests that the optical band gap of the TDCV-TPA can be more decreased with increasing molarity. As seen in Table 1, the obtained E_g values (1.916, 1.898 and 1.892 eV) from the plot of $(\alpha h\nu)^{1/2}$ vs. E of the TDCV-TPA for 1, 2 and 3 mM are close to values (1.920, 1.890, 1887 eV) of the first decrease (at 646, 656 and 657 nm) of transmittance spectra of the TDCV-TPA for 1, 2 and 3 mM, respectively. Similarly, the obtained E_g values (1.916, 1.898 and 1.892 eV) from the plot of $(\alpha h\nu)^{1/2}$ vs. E of the TDCV-TPA for 1, 2 and 3 mM are close to values (1.902, 1.882, 1882 eV) of the absorption band edge of the TDCV-TPA for 1, 2 and 3 mM, respectively.

There is a research [27] on too few optical parameters of the TDCV-TPA film deposited onto glass, but, there is not any report in the literature about the detailed optical properties of the *solutions* of the TDCV-TPA by a solution technique. We claim that this solution technique for investigation of the optical properties of the soluble materials is cheaper and more accurate than a film technique. This situation is originated from deposition devices such as spin-coater, Langmuir–Blodgett (LB) devices, which are more expensive devices (there is not need to any deposition devices for optical properties) and various impurities may occur on the surface of the film, prior, during and after the coating of a film. These disadvantages adversely affect the optical properties of the material. Thus, as given in Section 3.1., we investigated the surface morphology properties of the TDCV-TPA film to describe the roughness parameters such as roughness average, root mean square roughness, surface skewness, and surface kurtosis and AFM images (the light and dark regions, homogeneous/inhomogeneous distribution, valley regions (pits), deeps of the pits, depressions and porous/turned surface, spiky/bumpy/perfectly random surfaces, ratio of *sq* to *sa* of the TDCV-TPA film), because these roughness parameters and AFM images affected optical properties of the TDCV-TPA material. If these roughness parameters and AFM images obtained are not exactly as expected parameters/conditions, these disadvantages adversely affect the optical properties of the material. Hence, we can claim that this solution technique for investigation of the optical properties of the soluble materials is more accurate than a film technique.

3.3. The optical properties of the solutions of the TDCV-TPA for lower molarities

The absorbance (*Abs*) spectras of the solutions of the TDCV-TPA were taken to investigate their optical properties for 0.33, 0.12, 0.05, 0.024 and 0.010 mM of the lower molarities and the plot of the *Abs* vs. λ is shown in Fig. 6. As seen in Fig. 6, the absorbance values of the solutions of the TDCV-TPA exist almost in the near ultraviolet (200–380 nm) and visible region (380–780 nm). This shows that the near ultraviolet and visible regions are very significant regions for the TDCV-TPA small-molecule semiconducting dye. As seen in Fig. 6, the uncertainty which results from the high molarity in the absorbance values of the solution of the TDCV-TPA for 1 mM in the range of about 260 and 580 nm is becoming gradually disappear with decreasing molarity and all the absorbance values of the TDCV-TPA can be clearly appeared after the molarity values of less than 0.05 mM. As seen in Fig. 6, the absorbance of the TDCV-TPA decreases with decreasing molarity. The maximum absorption wavelengths (λ_{max}) of the solutions of the TDCV-TPA for 0.024 and 0.010 mM were found to be 510 and 509 nm, respectively. It is observed that the Abs_{max} value of the solution of the TDCV-TPA obtained in the visible region. Then, the absorbance (Abs_{max}) values at maximum absorption wavelengths of the solutions of the TDCV-TPA for 0.024 and 0.010 mM were found to be 2.819 and 1.931, respectively. It is observed that the Abs_{max} value of the solution of the TDCV-TPA can be decreased with decreasing molarity. There is another interesting result, as seen in Fig. 6, the λ_{max} of the solution of the TDCV-TPA for 0.05 mM in the near ultraviolet region is observed, while the maximum absorption wavelength (λ_{max}) of the

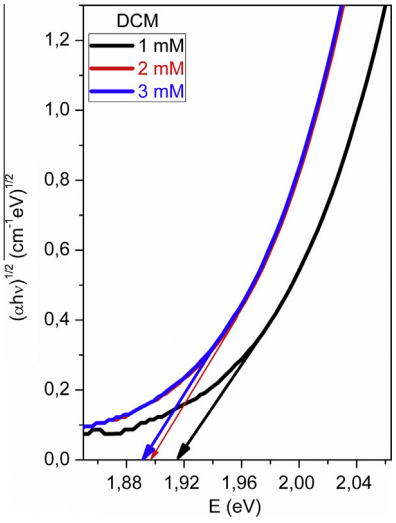

Fig. 5. The $(\alpha h\nu)^{1/2}$ plot vs. the photon energy (E) of the TDCV-TPA for 1, 2 and 3 mM.

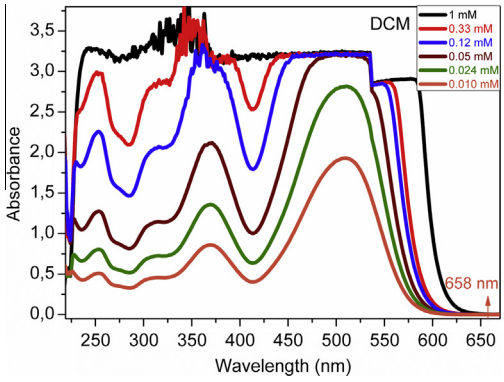

Fig. 6. The plot of the Absorbance vs. λ of the TDCV-TPA for 1, 0.33, 0.12, 0.05, 0.024 and 0.010 mM.

solution of the TDCV-TPA for 0.05 mM is not observed in the visible region. The λ_{max} values of the solutions of the TDCV-TPA for 0.05, 0.024 and 0.010 mM in the near ultraviolet region were found to be 371, 369 and 369 nm, respectively. Then, the Abs_{max} values at λ_{max} of the solutions of the TDCV-TPA for 0.05, 0.024 and 0.010 mM in the near ultraviolet region were found to be 2.122, 1.358 and 0.860, respectively. Finally, as seen in Fig. 6, the absorbance values of the solutions of the TDCV-TPA sharply decrease after λ_{max} value (at about 510 nm) and the red light of the TDCV-TPA is emitted about 658 nm. This situation is very significant and is prefered for high spectral optical/electrical/opto-electronic devices.

The molar extinction coefficient (ε) values of the solutions of the TDCV-TPA for 0.33, 0.12, 0.05, 0.024 and 0.010 mM were calculated from Eq. (1). The ε plot vs. λ of the solutions of the TDCV-TPA for 33, 0.12, 0.05, 0.024 and 0.010 mM is shown in Fig. 7. As seen in Fig. 7, the ε values of the solutions of the TDCV-TPA exist almost in the near ultraviolet and visible region. As seen in Fig. 7, the ε values of the TDCV-TPA can be clearly appeared after the molarity values of less than 0.05 mM. As seen in Fig. 7, the molar extinction coefficient of the TDCV-TPA increases with decreasing molarity. The maximum molar extinction coefficient (ε_{max}) values at λ_{max} values (510 and 509 nm) of the solutions of the TDCV-TPA for 0.024 and 0.010 mM were found to be 1.175×10^5 and 1.931×10^5 L mol^{-1} cm^{-1}, respectively. It is observed that the ε_{max} value of the solution of the TDCV-TPA can be increased with decreasing molarity. Also, as seen in Fig. 7, The ε values at λ_{max} (371, 369 and 369 nm) of the solutions of the TDCV-TPA for 0.05, 0.024 and 0.010 mM in the near ultraviolet region were found to be 5.646×10^4, 6.318×10^4 and 8.600×10^4 L mol^{-1} cm^{-1}, respectively. The ε values of the solutions of the TDCV-TPA sharply decrease after λ_{max} value (at about 510 nm). The mass extinction coefficients (α) can be calculated by [50].

$$\alpha = \frac{\varepsilon}{M_A} \tag{3}$$

where M_A is the molecular mass of the material, which is 719.86 g/mol of the TDCV-TPA semiconducting dye. The maximum mass extinction coefficient (α_{max}) values at ε_{max} values (1.175×10^5 and 1.931×10^5 L mol^{-1} cm^{-1}, respectively) of the solutions of the TDCV-TPA for 0.024 and 0.010 mM were found to be 163.226 and 268.247 L g^{-1} cm^{-1}, respectively. It is observed that the α_{max} value of the solution of the TDCV-TPA can be increased with decreasing molarity. The α values at λ_{max} (371, 369 and 369 nm) of the solutions of the TDCV-TPA for 0.05, 0.024 and 0.010 mM in the near ultraviolet region were found to be 78.432, 87.767 and 119.468 L g^{-1} cm^{-1}, respectively.

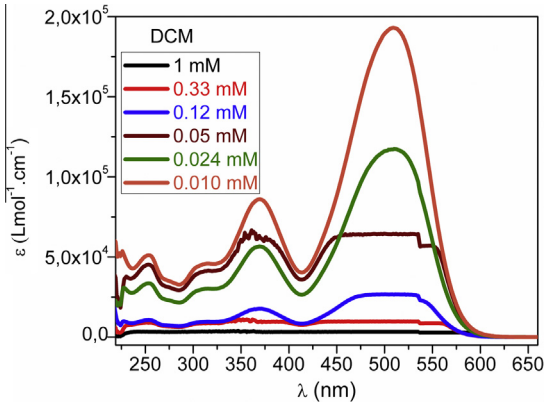

Fig. 7. The ε plot vs. λ of the solutions of the TDCV-TPA for 1, 33, 0.12, 0.05, 0.024 and 0.010 mM.

The transmittance spectras of the solutions of the TDCV-TPA were taken to investigate their optical properties for 0.33, 0.12, 0.05, 0.024 and 0.010 mM and the plot of the transmittance vs. λ is shown in Fig. 8a. As seen in Fig. 8a, the transmittance spectra of the solutions of the TDCV-TPA exist almost in the near ultraviolet and visible region and the transmittance of the TDCV-TPA increases with decreasing molarity. In the visible region, the average transmittance (T_{avg}) values of the solutions of the TDCV-TPA for 0.33, 0.12, 0.05, 0.024 and 0.010 mM were calculated and given in Table 2. As seen in Table 2, the T_{avg} (57.954%) for 0.010 mM is the highest, while the T_{avg} (41.292%) for 1 mM is the lowest. It is observed that the T_{avg} of the solutions of the TDCV-TPA in the visible region increases with decreasing molarity. To estimate the absorption band edge of the solutions of the TDCV-TPA, we plotted the curves of $dT/d\lambda$ vs. λ of the solutions of the TDCV-TPA for 0.33, 0.12, 0.05, 0.024 and 0.010 mM, as shown in Fig. 8b. As seen in Fig. 8b, there is a shift in the direction of the lower wavelengths with decreasing molarity and the absorption edge of the TDCV-TPA is shifted to lower wavelengths, which is due to the change in the band gap with molarity. In other words, the shifting towards lower wavelengths of the absorption edge is due to the increasing of optical band gap with decreasing molarity. The absorption band edge values of the solutions of the TDCV-TPA for 0.33, 0.12, 0.05, 0.024 and 0.010 mM were calculated from the maximum peak position and given in Table 2. As seen in Table 2, the maximum peak of the solutions of the TDCV-TPA varies from 652 to 612 nm with decreasing molarity. This result suggests that the absorption band edge of the solutions of the TDCV-TPA shifts from 1.902 to 2.026 eV, that is, the absorption band edge increases with the decreasing molarity.

To determine the optical band gap of the solutions of the TDCV-TPA for 0.33, 0.12, 0.05, 0.024 and 0.010 mM, the $(\alpha h\nu)^{1/2}$ plot vs. E of the TDCV-TPA is shown in Fig. 9. By extrapolating the linear plot to $(\alpha h\nu)^{1/2} = 0$, the E_g values of the TDCV-TPA for 0.33, 0.12, 0.05,

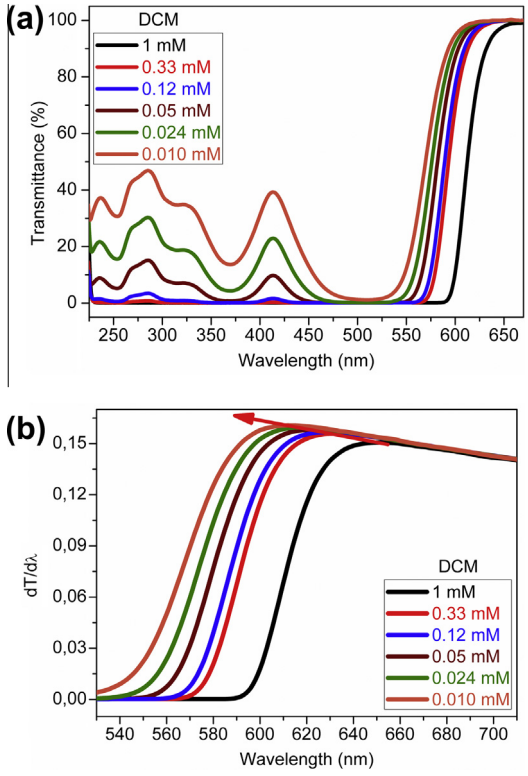

Fig. 8. (a) The plot of the transmittance vs. λ and (b) the curves of $dT/d\lambda$ vs. λ of the solutions of the TDCV-TPA for 1, 0.33, 0.12, 0.05, 0.024 and 0.010 mM.

Table 2
The T_{avg} (in the visible region), $\lambda_{max.peak}$, absorption band edge, E_g values of the solutions of the TDCV-TPA for 0.33, 0.12, 0.05, 0.024 and 0.010 mM.

Molarity (mM)	T_{avg} (%)	$\lambda_{max.peak}$ (nm)	Absorption band edge (eV)	E_g (eV)
0.33	46.340	631	1.965	1.950
0.12	47.433	629	1.971	1.962
0.05	49.976	623	1.990	1.979
0.024	53.229	617	2.010	1.993
0.010	57.954	612	2.026	2.008

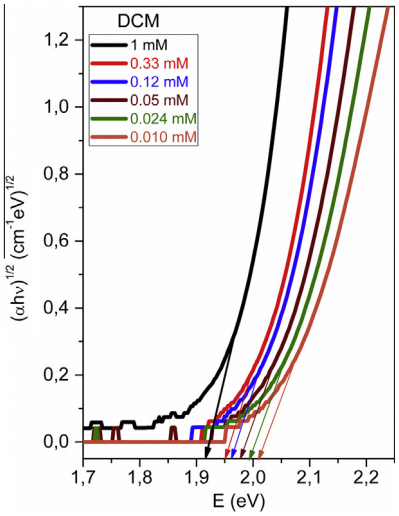

Fig. 9. The $(\alpha h\nu)^{1/2}$ plot vs. E of the TDCV-TPA for 1, 0.33, 0.12, 0.05, 0.024 and 0.010 mM.

0.024 and 0.010 mM were obtained and given in Table 2. As seen in Table 2, the E_g (1.916 eV) of the TDCV-TPA for 1 mM is the lowest of all the solutions, while the E_g (2.008 eV) of the TDCV-TPA for 0.010 mM is the highest. This suggests that the optical band gap of the TDCV-TPA can be more increased with decreasing molarity. As seen in Table 2, the obtained E_g values from the plot of $(\alpha h\nu)^{1/2}$ vs. E of the TDCV-TPA for 0.33, 0.12, 0.05, 0.024 and 0.010 mM are close to values of the absorption band edge and obtained especially E_g values of the first decrease of transmittance spectra of the TDCV-TPA for the same molarities. It is observed that the optical band gap E_g of the TDCV-TPA can be found from the plot of $(\alpha h\nu)^{1/2}$ vs. E, the absorption band edge and the first decrease of transmittance spectra of the TDCV-TPA.

The Angle of incidence $\Phi(B)$ is given [73–75].

$$\Phi(B) = \tan^{-1}\left(\frac{n_2}{b_1}\right) \tag{4}$$

The angle Φ_1 values of incidence of the solutions of the TDCV-TPA for 0.33, 0.12, 0.05, 0.024 and 0.010 mM were calculated from Eq. (4) (n_1: the refractive index of the medium, n_2: the refractive index of the solutions of the TDCV-TPA). The Φ_1 plot vs. E of the solutions of the TDCV-TPA is shown Fig. 10. As seen in Fig. 10, the angle Φ_1 values of incidence of the TDCV-TPA sharply increase with increasing photon energy in the range of about 1.83 and 2.30 eV and decrease with decreasing molarity. Similarly, the angle of refraction is calculated from well known Snell's law [76].

$$\Phi_2 = \sin^{-1}\left(\frac{n_1}{n_2}\sin\Phi_1\right) \tag{5}$$

The angle Φ_2 values of refraction of the solutions of the TDCV-TPA for 0.33, 0.12, 0.05, 0.024 and 0.010 mM were calculated from Eq. (5) and the Φ_2 plot vs. E of the TDCV-TPA for 0.33, 0.12, 0.05, 0.024 and 0.010 mM is shown Fig. 10. As seen in Fig. 10, the angle

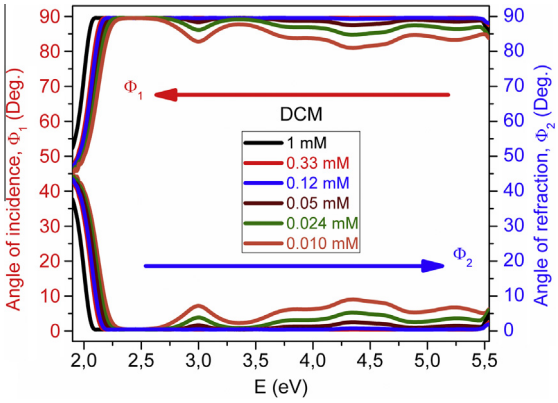

Fig. 10. The Φ_1 and Φ_2 plot vs. E of the solutions of the TDCV-TPA for 1, 0.33, 0.12, 0.05, 0.024 and 0.010 mM.

Φ_2 values of refraction of the TDCV-TPA sharply decrease with increasing photon energy in the range of about 1.83 and 2.30 eV and increase with decreasing molarity. Also, the angle Φ_1 values of incidence of the solutions of the TDCV-TPA are higher than the angle Φ_2 values of refraction of the solutions of the TDCV-TPA. This situation attributes to the refractive index (n_2) of the solutions of the TDCV-TPA is higher than the refractive index (n_1) of the medium.

The complex dielectric constant is described as,

$$\hat{\varepsilon} = \varepsilon_1 + i\varepsilon_2 = \hat{\varepsilon}^2 = (n \pm ik)^2 = (n^2 - k^2) + i2nk \tag{6}$$

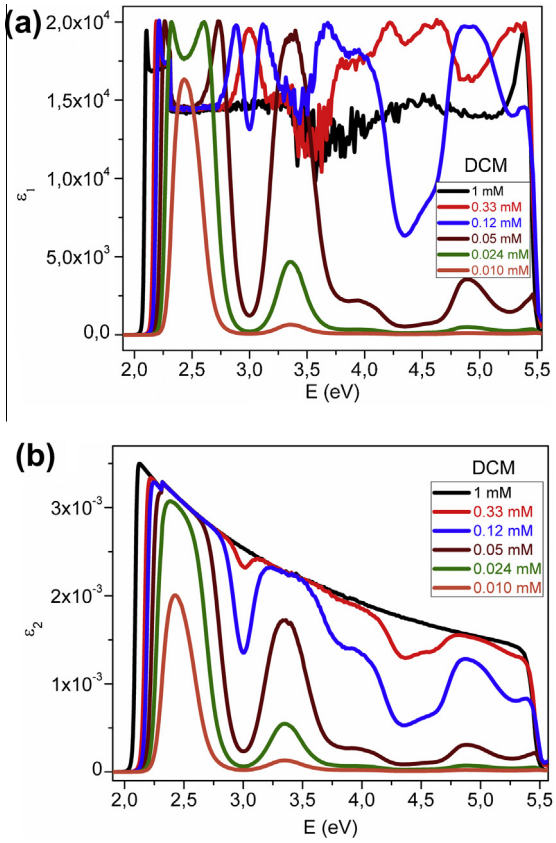

Fig. 11. The (a) real and (b) imaginary parts of dielectric constant dependence on photon energy of the TDCV-TPA for 1, 0.33, 0.12, 0.05, 0.024 and 0.010 mM.

where ε_1 is the real part and ε_2 is the imaginary of the dielectric constant. The imaginary and real parts of dielectric constant are given as [74,75]

$$\varepsilon_1 = n^2 - k^2 \tag{7}$$

and

$$\varepsilon_2 = 2nk \tag{8}$$

where $k = \alpha\lambda/4\pi$. Fig. 11a and b shows the real and imaginary parts of dielectric constant dependence on photon energy of the TDCV-TPA for 0.33, 0.12, 0.05, 0.024 and 0.010 mM, respectively. As seen in Fig. 11a, the uncertainty, which results from the high molarity, in the plot of the real part (ε_1) of dielectric constant values of the solution of the TDCV-TPA for 1 mM in the range of about 2.13 and 4.8 eV is becoming gradually disappear with decreasing molarity and all the ε_1 values of the TDCV-TPA can be clearly appeared after the molarity values of less than 0.05 mM. As seen in Fig. 11a, the real part of dielectric constant of the TDCV-TPA decreases with decreasing molarity. The real part of dielectric constant of the TDCV-TPA is composed normal and anomalous (or abnormal) dispersion regions. The ε_1 values of the TDCV-TPA increase with increasing photon energy (or frequency) in normal dispersion region, while the ε_1 values of the TDCV-TPA decrease with increasing photon energy (or frequency) in anomalous (or abnormal) dispersion region. The abnormal (anomalous) behaviors of the TDCV-TPA are owing to the resonance effect between the electronspolarization and the incident electromagnetic radiation [12], which leads to the coupling of electrons in solutions of the TDCV-TPA to the oscillating electric field. As seen in Fig. 11b, the imaginary part ε_2 values of dielectric constant of the TDCV-TPA can be clearly appeared after the molarity values of less than 0.05 mM and the ε_2 values of the TDCV-TPA decrease with decreasing molarity. As seen in Fig. 11a and b the real part of dielectric constant of the TDCV-TPA is higher than that of the imaginary part of dielectric constant of the TDCV-TPA.

The electrical susceptibility associated with electron transitions from band i to band j is expressed as [77,78].

$$\chi_v = \frac{e^2}{4\pi^2 m}\sum_k \frac{f_{jik}}{v_{jik}^2 - v^2} \tag{9}$$

where k is the wave number vector, hv_{jik} is the energy difference between the state k in band i and the state k in band j and f_{jik} is the oscillator strength for this transition. The electrical susceptibility due to the intraband transitions of free carriers can be obtained from the optical constants and it is determined as [77,79].

$$\chi_c = \frac{1}{4\pi}(n^2 - k^2 - \varepsilon_o) \tag{10}$$

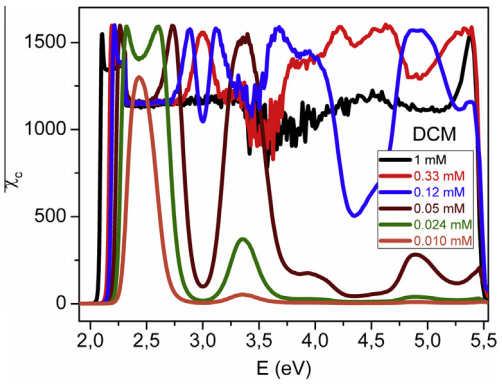

Fig. 12. The plot of the electric susceptibility (χ_c) vs. E of the solutions of the TDCV-TPA for 1, 0.33, 0.12, 0.05, 0.024 and 0.010 mM.

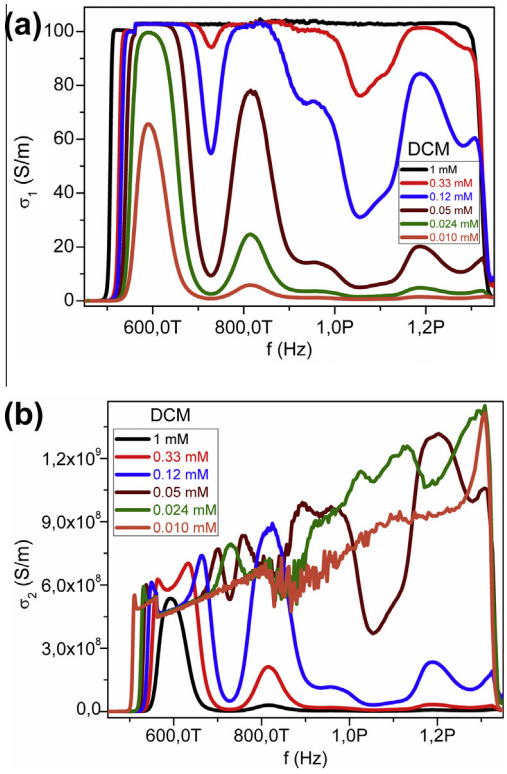

Fig. 13. The (a) real and (b) imaginary part of the optical conductivity dependence on frequency of the TDCV-TPA for 1, 0.33, 0.12, 0.05, 0.024 and 0.010 mM.

where ε_o is the dielectric constant in the absence of any contribution from free carriers. The electric susceptibility of the solutions of the TDCV-TPA for 0.33, 0.12, 0.05, 0.024 and 0.010 mM dependence on E is shown in Fig. 12. As seen in Fig. 12, the plot of the electric susceptibility (χ_c) of the TDCV-TPA is similar to the ε_1 plot vs. E of the TDCV-TPA and the electric susceptibility (χ_c) of the TDCV-TPA decreases with decreasing molarity.

The optical properties of the solution of the TDCV-TPA can be analyzed by a complex optical conductivity [73–75].

$$\sigma(\omega) = \sigma_1(\omega) + i\sigma_2(\omega) \tag{11}$$

where σ_1 is the real part of conductivity and σ_2 is the imaginary part of conductivity. The real and imaginary parts of the optical conductivity dependence on frequency of the TDCV-TPA for 0.33, 0.12, 0.05, 0.024 and 0.010 mM are shown in Fig. 13a and b, respectively. As seen in Fig. 13a, the real part (σ_1) of the optical conductivity of the TDCV-TPA changes with increasing frequency and decreases with decreasing molarity. As seen in Fig. 13b, all the σ_2 values of the TDCV-TPA can be clearly appeared after the molarity values of less than 0.05 mM and the σ_2 of the TDCV-TPA decreases with decreasing molarity. As seen in Fig. 13a and b, the imaginary parts of the optical conductivity of the TDCV-TPA are higher than that of the real parts of the optical conductivity.

3.4. The effects of the solvents on optical properties of the solutions of the TDCV-TPA

The *Abs.* spectras of the solutions of the TDCV-TPA were taken to investigate their optical properties for 2, 0.28 and 0.12 mM of the dichloromethane (DCM) and chloroform solvents. As seen in Fig. 2a and b, the color[1] of the solution of the TDCV-TPA dissolved in DCM is more darker (dark red) than that of the color (light red)

[1] For interpretation of color in Fig. 2, the reader is referred to the web version of this article.

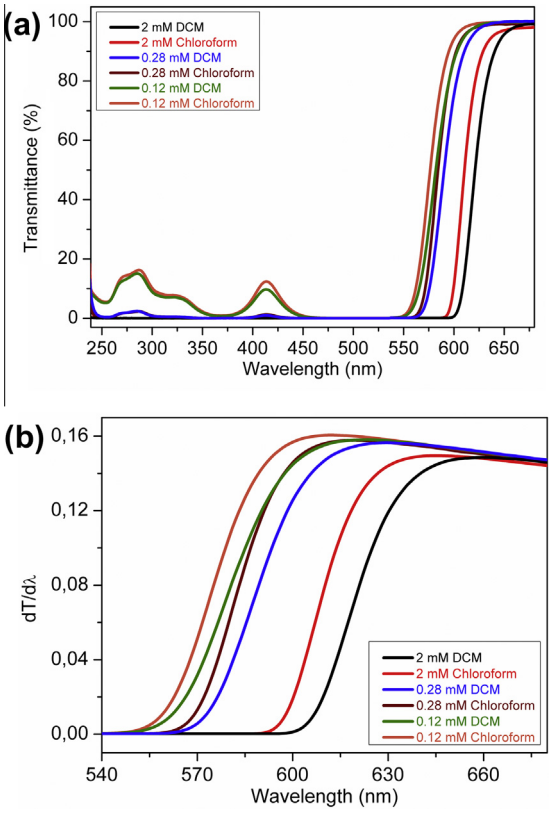

Fig. 14. (a) The plot of the transmittance vs. λ and (b) the curves of $dT/d\lambda$ vs. λ of the solutions of the TDCV-TPA for 2, 0.28 and 0.12 mM of the Dichloromethane (DCM) and chloroform solvents.

dissolved in chloroform. This is a significant effect on the optical properties of the TDCV-TPA semiconducting dye, because the color of any material affects the optical measurements. Absorbance value of the darker colored solution of any material is higher than that of the less darker colored solution of the same material.

The molar extinction coefficient (ε) values of the solutions of the TDCV-TPA for 2, 0.28 and 0.12 mM of the DCM and chloroform solvents were calculated from Eq. (1). The maximum molar extinction coefficient (ε_{max}) values at λ_{max} of the solutions of the TDCV-TPA for 2, 0.28 and 0.12 mM of the DCM and chloroform solvents in the visible region are not observed because of high molarity. The ε_{max} values at λ_{max} (at 371 and 368 nm, respectively) of the TDCV-TPA for 0.12 mM of the DCM and chloroform solvents in the near ultraviolet region were found to be 1.768×10^4 and 1.713×10^4 L mol^{-1} cm^{-1}, respectively. It is observed that the ε_{max} value at λ_{max} of the TDCV-TPA for DCM solvent in the near ultraviolet region is higher than that of the value for chloroform and the ε_{max} value of the solution of the TDCV-TPA can be increased with decreasing molarity. The α_{max} values at ε_{max} values (1.768×10^4 and 1.713×10^4 L mol^{-1} cm^{-1}, respectively) of the solutions of the TDCV-TPA for 0.12 mM of the DCM and chloroform solvents in the near ultraviolet region were found to be 24.560 and 23.796 L g^{-1} cm^{-1}, respectively. It is observed that the α_{max} value at ε_{max} of the TDCV-TPA for DCM solvent in the near ultraviolet region is higher than that of the value for chloroform.

The plot of the transmittance of the solutions of the TDCV-TPA for 2, 0.28 and 0.12 mM of the DCM and chloroform solvents vs. λ is shown in Fig. 14a. As seen in Fig. 14a, the transmittance spectras of the solutions of the TDCV-TPA exists almost in the near ultraviolet and visible region and the transmittance of the TDCV-TPA increases with decreasing molarity. In the visible region, the T_{avg} values of the solutions of the TDCV-TPA for 2, 0.28 and 0.12 mM of the DCM and chloroform solvents were calculated and given in Table 3. As seen in Table 3, the T_{avg} values (49.976 and 51.584%)) for 0.12 mM of the DCM and chloroform are the highest values, while the T_{avg} values (39.164 and 41.207%) for 2 mM of the DCM and chloroform are the lowest values. They are observed that the T_{avg} values of the solutions of the TDCV-TPA in the visible region increase with decreasing molarity and the T_{avg} values of the solutions of the TDCV-TPA for chloroform in the visible region are higher than that of the values of the TDCV-TPA for DCM in the visible region. To estimate the absorption band edge of the solutions of the TDCV-TPA, we plotted the curves of $dT/d\lambda$ vs. λ of the solutions of the TDCV-TPA for 2, 0.28 and 0.12 mM of the DCM and chloroform solvents, as shown in Fig. 14b. As seen in Fig. 14b, there is a shift in the direction of the lower wavelengths with decreasing molarity. The absorption band edge values of the solutions of the TDCV-TPA for 2, 0.28 and 0.12 mM of the DCM and chloroform solvents were calculated from the maximum peak position and given in Table 3. As seen in Table 3, the maximum peak for DCM varies from 659 to 621 nm, while the maximum peak for chloroform varies from 645 to 612 nm with decreasing molarity. These results suggest that the absorption band edge for DCM shifts from 1.882 to 1.997 eV, while the absorption band edge for chloroform shifts from 1.923 to 2.027 eV, that is, the absorption band edge increases with the decreasing molarity and the absorption band edge values for DCM is lower than that of the values of the same molarities of chloroform.

To determine the E_g of the solutions of the TDCV-TPA for 2, 0.28 and 0.12 mM of the DCM and chloroform solvents, the $(\alpha h\nu)^{1/2}$ plot vs. E of the TDCV-TPA is shown in Fig. 15. The E_g values of the TDCV-TPA for 2, 0.28 and 0.12 mM of the DCM and chloroform were obtained and given in Table 3. As seen in Table 3, the E_g values (1.898 and 1.920 eV, respectively) of the TDCV-TPA for 2 mM of the DCM and chloroform are the highest values, while the E_g values (1.977 and 2.009 eV, respectively) of the TDCV-TPA for 0.12 mM of the DCM and chloroform are the lowest values. These results suggest that the optical band gap of the TDCV-TPA increases with the decreasing molarity and the E_g values for DCM are lower than that of the values for the same molarities with chloroform and the obtained E_g values of the TDCV-TPA are lower than that of the obtained E_g values of the TDCV-TPA. Thus, to obtain lower optical energy-gap of the TDCV-TPA can be prefered DCM solvent. As seen in Table 3, the obtained E_g values from the plot of $(\alpha h\nu)^{1/2}$ vs. E of the TDCV-TPA for 2, 0.28 and 0.12 mM of the DCM and chloroform are close to values of the absorption band edge and obtained especially E_g values of the first decrease of transmittance spectra of the

Table 3
The T_{avg} (in the visible region), $\lambda_{max.peak}$, absorption band edge, E_g values of the solutions of the TDCV-TPA for 2, 0.28 and 0.12 mM of the Dichloromethane (DCM) and chloroform solvents.

Dichloromethane (DCM)					Chloroform			
Molarity (mM)	T_{avg} (%)	$\lambda_{max.peak}$ (nm)	Absorption band edge (eV)	E_g (eV)	T_{avg} (%)	$\lambda_{max.peak}$ (nm)	Absorption band edge (eV)	E_g (eV)
2	39.164	659	1.882	1.898	41.207	645	1.923	1.920
0.28	47.140	623	1.990	1.955	49.976	620	2.000	1.987
0.12	49.976	621	1.997	1.977	51.584	612	2.027	2.009

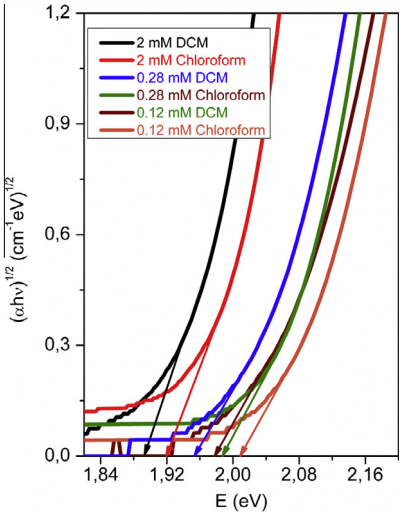

Fig. 15. The $(\alpha h\nu)^{1/2}$ plot vs. E of the TDCV-TPA for 2, 0.28 and 0.12 mM of the dichloromethane (DCM) and chloroform solvents.

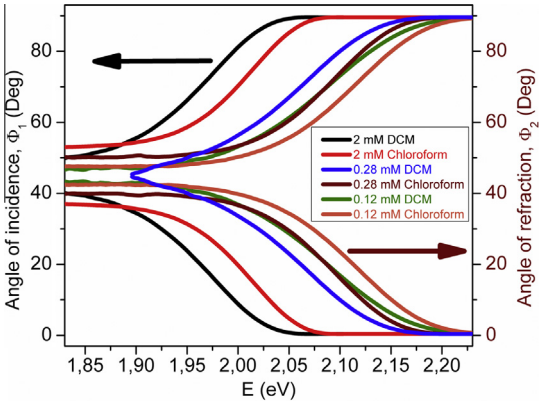

Fig. 16. The Φ_1 and Φ_2 plot vs. E of the solutions of the TDCV-TPA for 2, 0.28 and 0.12 mM of the dichloromethane (DCM) and chloroform solvents.

TDCV-TPA for the same solvent and molarities. This suggests that the E_g of the TDCV-TPA can be found from the plot of $(\alpha h\nu)^{1/2}$ vs. E, the absorption band edge and the first decrease of transmittance spectra of the TDCV-TPA.

The Φ_1 and Φ_2 values of the TDCV-TPA for 2, 0.28 and 0.12 mM of the DCM and chloroform were calculated from Eqs. (4) and (5), respectively. The Φ_1 and Φ_2 plot vs. E of the TDCV-TPA is shown Fig. 16. As seen in Fig. 16, the Φ_1 values of the TDCV-TPA sharply increase with increasing photon energy in the range of about 1.83 and 2.23 eV and decrease with decreasing molarity, while the Φ_2 values of the TDCV-TPA sharply decrease with increasing photon energy in the range of about 1.83 and 2.23 eV and increase with decreasing molarity. The Φ_1 values for DCM are higher than that of the values for chloroform, while the Φ_2 values for DCM are lower than that of the values for chloroform. Also, the Φ_1 values of the TDCV-TPA are higher than the Φ_2 values of the TDCV-TPA. This situation attributes to the refractive index (n_2) of the solutions of the TDCV-TPA is more higher than the refractive index (n_1) of the medium.

4. Conclusion

The AFM images of the TDCV-TPA film have the light, dark and valley regions (pits). The ratio (1.267) of *sq* to *sa* of the TDCV-TPA film is reasonably close to the value of 1.25 predicted by theory. The TDCV-TPA film indicated the low valleys with bumpy surface. The molar extinction coefficient, optical band gap, angle values of refraction of the TDCV-TPA decrease with increasing molarity, while the absorbance at maximum absorption wavelengths, angle of incidence, electric susceptibility, real part values of the optical conductivity of the TDCV-TPA increase with increasing molarity. The obtained E_g values (1.916, 1.898 and 1.892 eV) from the plot of $(\alpha h\nu)^{1/2}$ vs. E of the TDCV-TPA for 1, 2 and 3 mM are close to values (1.902, 1.882, 1882 eV) of the absorption band edge of the TDCV-TPA for 1, 2 and 3 mM, respectively. The absorption band edge values for DCM are lower than that of the values of the same molarities of chloroform.

Acknowledgments

This work was supported by The Management Unit of Scientific Research Projects of Muş Alparslan University (MUSBAP) under Project 0001. The author is grateful to Mrs. Hilal Gözler who is R&D Scientist and Nanomagnetic Instruments Co. because of helping with the AFM measurements.

References

[1] M. Pope, C.E. Swenberg, Electronic Processes in Organic Crystals, Oxford University Press, New York, 1982.
[2] B. Park, Electronic and Structural Properties of Pentacene at Organic/Inorganic Interfaces, University of Wisconsin-Madison, 2008.
[3] B. Gunduz, I.S. Yahia, F. Yakuphanoglu, Electrical and photoconductivity properties of p-Si/P3HT/Al and p-Si/P3HT:MEH-PPV/Al organic devices: Comparison study, Microelectron. Eng. 98 (2012) 41–57.
[4] H.S. Nalwa (Ed.), Handbook of Conductive Molecules and Polymers, vol. 1–4, Wiley, Chichester, UK, 1997.
[5] A. Cravino, P. Leriche, O. Alévêque, S. Roquet, J. Roncali, Light-emitting organic solar cells based on a 3d conjugated system with internal charge transfer, Adv. Mater. 18 (2006) 3033–3037.
[6] C.D. Dimitrakopolous, P. Malenfant, Organic thin film transistors for large area electronics, Adv. Mater. 14 (2002) 99–117.
[7] J.A. Rogers, Z. Bao, K. Baldwin, A. Dodabalapur, B. Crone, V.R. Raju, V. Kuck, H. Katz, K. Ammundson, J. Ewing, P. Drzaic, Paper-like electronic displays: large-area rubber-stamped plastic sheets of electronics and microencapsulated electrophoretic inks, Proc. Natl. Acad. Eng. 98 (9) (2001) 4835–4840.
[8] F. Garnier, Organic-Based Electronics à la Carte, Acc. Chem. Res. 32 (1999) 209–215.
[9] G. Horowitz, Organic field-effect transistors, Adv. Mater. 10 (5) (1998) 365–377.
[10] J.H. Burroughs, D.D.C. Bradley, A.B. Brown, R.N. Marks, K. Mackay, R.H. Friend, P.L. Burn, A.B. Holmes, Light-emitting diodes based on conjugated polymers, Nature 347 (1990) 539–541.
[11] A. Kraft, A.C. Grimsdale, A.B. Holmes, Electroluminescent conjugated polymers – seeing polymers in a new light, Angew. Chem. Int. Ed. 37 (1998) 402–428.
[12] U. Mitschke, P. Bäuerle, The electroluminescence of organic materials, J. Mater. Chem. 10 (2000) 1471–1507.
[13] S.S. Sun, N.S. Sariciftci, Organic Photovoltaics - Mechanism, Materials, and Devices, CRC Press, Boca Raton, FL, 2005.
[14] C.J. Brabec, V. Dyakonov, J. Parisi, N.S. Sariciftci, Organic Photovoltaics: Concepts and Realisation, Springer Verlag, Berlin, 2003.
[15] C.J. Brabec, N.S. Sariciftci, J.C. Hummelen, Plastic solar cells, Adv. Funct. Mater. 11 (2001) 15–26.
[16] P. Peumans, A. Yakimov, S.R. Forrest, Small molecular weight organic thin-film photodetectors and solar cells, J. Appl. Phys. 93 (2003) 3693–3723.
[17] F. Yakuphanoglu, B. Gunduz, Effects of channel widths, thicknesses of active layer on the electrical and photosensing properties of the 6,13-bis(triisopropylsilylethynyl) pentacene transistors by thermal evaporation method: Comparison study, Synth. Met. 162 (2012) 1210–1239.
[18] C.D. Dimitrakopoulos, P.R.L. Malenfant, Organic thin film transistors for large area electronics, Adv. Mater. 14 (2002) 99–117.
[19] A.A.M. Farag, B. Gunduz, F. Yakuphanoglu, W.A. Farooq, Controlling of electrical characteristics of Al/p-Si Schottky diode by tris(8-hydroxyquinolinato) aluminum organic film, Synth. Met. 160 (2010) 2559–2563.
[20] Lei Diao, C. Daniel Frisbie, D.D. Schroepfer, P. Paul Ruden, Electrical characterization of metal/pentacene contacts, J. Appl. Phys. 101 (2007) 014510–014517.
[21] A. Rouis, C. Dridi, I. Dumazet-Bonnamour, J. Davenas, H. Ben Ouada, Transport mechanism and trap distribution in ITO/azo-calix[4]arene derivative/Al diode structure, Phys. B 399 (2007) 109–115.
[22] G. Harsaanyi, Polymer films in sensor applications: a review of present uses and future possibilities, Sensor Rev. 20 (2000) 98–105.

[23] J.M. Shaw, P.F. Seidler, Organic electronics: introduction, IBM J. Res. Dev. 45 (2001) 3–9.
[24] R. Ben Chaabane, A. Ltaief, C. Dridi, H. Rahmouni, A. Bouazizi, H. Ben Ouada, Study of organic thin film transistors based on nickel phthalocyanine: effect of annealing, Thin Solid Films 427 (2003) 371–376.
[25] C. Reese, M. Roberts, M.M. Ling, Z. Bao, Organic thin film transistors, Mater. Today 7 (9) (2004) 20–27.
[26] C. Kim, K. Bang, I. An, C.J. Kang, Y.S. Kim, D. Jeon, Morphology and ellipsometry study of pentacene films grown on native SiO_2 and glass substrates, Curr. Appl. Phys. 6 (2006) 925–930.
[27] K. Sulaiman, M.S. Fakir, Electrical conduction and photovoltaic effects of TPA-derivative solar cells, Thin Solid Films 519 (2011) 5219–5222.
[28] Y. Shirota, Photo- and electroactive amorphous molecular materials – molecular design, syntheses, reactions, properties, and applications, J. Mater. Chem. 15 (2005) 75–93.
[29] M.M. Stylianakis, J.A. Mikroyannidis, Q.F. Dong, J.N. Pei, Z.Y. Liu, W.J. Tian, Synthesis, photophysical and photovoltaic properties of star-shaped molecules with triphenylamine as core and phenylethenylthiophene or dithienylethylene as arms, Sol. Energy Mater. Sol. Cells 93 (2009) 1952–1958.
[30] Min Zhang, Zhanghua Wu, Quan Wang, Qijun Song, Yuqiang Ding, Synthesis and properties of a new [60] fullerene-donor system containing dicyanovinyl groups, Mater. Lett. 64 (2010) 2244–2246.
[31] Y.J. Shirota, Organic materials for electronic and optoelectronic devices, Mater Chem. 10 (1) (2000) 1–25.
[32] K. Walzer, B. Maennig, M. Pfeiffer, K. Leo, Highly efficient organic devices based on electrically doped transport layers, Chem. Rev. 107 (2007) 1233–1271.
[33] H.P. Zeng, T.T. Wang, S.D. Sandanayaka, Y. Araki, O.J. Ito, Photoinduced charge separation and charge recombination in [60]fullerene-ethylcarbazole and [60]fullerene-triphenylamines in polar solvents, J. Phys. Chem. A 109 (2005) 4713–4720.
[34] Y. Shirota, H. Kageyama, Charge carrier transporting molecular materials and their application in devices, Chem. Rev. 107 (2007) 953–1010.
[35] S. Roquet, A. Cravino, P. Leriche, O. Alévêque, P. Frère, J. Roncali, Triphenylamine-thienylenevinylene hybrid systems with internal charge transfer as donor materials for heterojunction solar cells, J. Am. Chem. Soc. 128 (2006) 3459–3466.
[36] A. Heredia, C.C. Bui, U. Suter, P. Young, T.E. Schaffer, Elastic properties of myelinated and de-myelinated mouse peripheral axons by atomic force microscopy, NeuroImage 37 (2007) 1218–1226.
[37] B. Rajesh Kumar, T. Subba Rao, AFM Studies on surface morphology, topography and texture of nanostructured zinc aluminum oxide thin films, Digest J. Nanomater. Biostruct. 7 (4) (2012) 1881–1889.
[38] D.D. Nesheva, E. Vateva, Z. Levi, D. Arsova, Thin film semiconductor nanomaterials and nanostructures prepared by physical vapour deposition: an atomic force microscopy study, J. Phys. Chem. Solids 68 (2007) 675–680.
[39] D. Marchetto, A. Rota, L. Calabri, G.C. Gazzadi, C. Menozzi, S. Valeri, AFM investigation of tribological properties of nano-patternedsiliconsurface, Wear 265 (2008) 577–582.
[40] N. Jalili, K. Laxminarayana, A review of atomic force microscopy imaging systems: application to molecular metrology and biological sciences, Mechatronics 14 (2004) 907–945.
[41] M. Kwoka, L. Ottaviano, J. Szuber, AFM study of the surface morphology of L-CVD SnO_2 thin films, Thin Solid Films 515 (2007) 8328–8331.
[42] K.R. Nagabhushana, B.N. Lakshminarasappa, K. Narasimha Rao, F. Singh, I. Sulania, AFM and photoluminescence studies of swift heavy ion induced nanostructured aluminum oxide thin films, Nucl. Instr. Meth. Phys. Res. B 266 (2008) 1049.
[43] N. Gizli, Morphological characterization of cellulose acetate based reverse osmosis membranes by Atomic Force Microscopy (FM) effect of evaporation time, Chem. Chem. Technol. 5 (3) (2011) 327–331.
[44] D. Ahn, S.-L. Chuang, Calculation of linear and nonlinear intersubband optical absorption in a quantum well model with an applied electric field, IEEE J. Quantum Electron. 23 (1987) 2196–2204.
[45] E.M. Goldys, J.J. Shi, Linear and nonlinear intersubband optical absorption in a strained double barrier quantum well, Phys. Status Solidi B 210 (1998) 237–248.
[46] H.M. Baghramyan, M.G. Barseghyan, A.A. Kirakosyan, R.L. Restrepo, C.A. Duque, Linear andnonlinearopticalabsorptioncoefficientsinGaAs/Ga1xAlxAs concentric double quantum rings: Effects of hydrostatic pressure and aluminum concentration, J. Lumin. 134 (2013) 594–599.
[47] R.F. Kazarinov, R.A. Suris, Possibility of the amplification of electromagnetic waves in a semiconductor with a superlattice, Sov. Phys. Semicond. 5 (1971) 707–709.
[48] D.A.B. Miller, Quantum-well optoelectronic switching devices, Int. J. High Speed Electron. Syst. 1 (1990) 19–46.
[49] T.H. Hood, Multiple quantum well (MQW) waveguide modulators, J. Lightwave Technol. 6 (1988) 743–757.
[50] Y. Li, N. Scales, R.E. Blankenship, R.D. Willows, M. Chen, Extinction coefficient for red-shifted chlorophylls: Chlorophyll d and chlorophyll f, Biochim. Biophys. Acta 2012 (1817) 1292–1298.
[51] R.C. Weast, M.J. Astle, W.H. Beyer, Definition, in: R.C. Weast, M.J. Astle, W.H. Beyer (Eds.), Handbook of Chemistry and Physics, CRC Press, Cleveland, 1988, p. F84.
[52] G.D. Fasman, Molar absorptivity and values for proteins at selected wavelength of the ultraviolent and visible region, in: G.D. Fasman (Ed.), Practical Handbook of Biochemistry and Molecular Biology, CRC Press, Cleveland, 1989, p. 196.
[53] A. Beer, Determination of the absorption of red light in colored liquids, Ann. Phys. 86 (1852) 78–88.
[54] M.S. Zakerhamidi, A. Ghanadzadeh, M. Moghadam, Solvent effects on the UV/visible absorption spectra of some aminoazobenzene dyes, Chem. Sci. Trans. 1 (1) (2012) 1–8.
[55] T. Fox, N. Rosch, The calculation of solvatochromic shifts: the n-$\pi*$ transition of acetone, Chem. Phys. Lett. 191 (1992) 33–37.
[56] C. Reichardt, Solvents and Solvent Effects in Organic Chemistry, Second edition, VCH, Weinheim, 1988.
[57] J. Catalán, J.P. Catalán, On the solvatochromism of the $n \leftrightarrow \pi*$ electronic transitions in ketones, Phys. Chem. Chem. Phys. 13 (2011) 4072–4082.
[58] S.E. DeBolt, P.A. Kollman, A theoretical examination of solvatochromism and solute-solvent structuring in simple alkyl carbonyl compounds. Simulations using statistical mechanical free energy perturbation methods, J. Am. Chem. Soc. 112 (1990) 7515–7524.
[59] M. Rossberg, W. Lendle, G. Pfleiderer, A. Tögel, E.L. Dreher, E. Langer, H. Rassaerts, P. Kleinschmidt, H. Strack, R. Cook, U. Beck, K.A. Lipper, T.R. Torkelson, E. Löser, K.K. Beutel, T. Mann, Chlorinated Hydrocarbons in Ullmann's Encyclopedia of Industrial Chemistry, Wiley-VCH, Weinheim, 2006.
[60] D.D. Perrin, W.L.F. Armarego, Purification of Laboratory Chemicals, Pergamon Press, Oxford, 2009.
[61] J.C. Bernede, L. Cattin, M. Makha, V. Jeux, P. Leriche, J. Roncali, V. Froger, M. Morsli, M. Addou, MoO3/CuI hybrid buffer layer for the optimization of organic solar cells based on a donor–acceptor triphenylamine, Sol. Energy Mater. Sol. Cells 110 (2013) 107–114.
[62] H. Zhang, J. Fan, Z.R. Iqbal, D.B. Kuang, L. Wang, H. Meier, D. Cao, Novel dithieno[3,2-b:20,30-d]pyrrole-based organic dyes with high molar extinction coefficient for dye-sensitized solar cells, Org. Electron. 14 (2013) 2071–2081.
[63] A.A.M. Farag, A. Ashery, M.A. Shenashen, Optical absorption and spectrophotometric studies on the optical constants and dielectric of poly (o-toluidine) (POT) films grown by spin coating deposition, Phys. B 407 (2012) 2404–2411.
[64] S.E. Fritz, T.W. Kelley, C.D. Frisbie, Effect of dielectric roughness on performance of pentacene TFTs and restoration of performance with a polymeric smoothing layer, J. Phys. Chem. B 109 (2005) 10574–10577.
[65] H.C. Ward, Chapter IV: Profile Characterization, Rough Surfaces, T.R. Thomas Ed, Longman, London, 1982.
[66] A.M. Vilas, J.M. Bruque, M.L. Gonzalez-Martin, Sensitivity of surface roughness parameters to changes in the density of scanning points in multi-scale AFM studies, Appl. Biomater. Surf. Ultramicrosc. 107 (2007) 617–625.
[67] J. Tauc, A. Menth, States in the gap, J. Non-Cryst. Solids 8–10 (1972) 569–585.
[68] S. Bhadra, N.K. Singha, D. Khastgir, Effect of aromatic substitution in aniline on the properties of polyaniline, Eur. Polymer J. 44 (2008) 1763–1770.
[69] W. Feng, Z. Qi, Y. Sun, Synthesis and characterization of novel two-component conjugated polythiophenes with 3-octyl and 3-isooctylthiophene side chains, J. Appl. Polym. Sci. 104 (2007) 1169–1175.
[70] V. Bavastrello, S. Carrara, M.K. Ram, N. Nicolini, Optical and electrochemical properties of poly(ortho-toluidine) – multi walled carbon nanotubes composite langmuir-schaefer films, Langmuir 20 (2004) 969–973.
[71] B. Sankaran, J.R. Reynolds, High-contrast electrochromic polymers from alkyl-derivatized poly(3,4-ethylenedioxythiophenes), Macromolecules 30 (1997) 2582–2588.
[72] K. Colladet, M. Nicolas, L. Goris, L. Lutsen, D. Vanderzande, Low-band gap polymers for photovoltaic applications, Thin Solid Films 451–452 (2004) 7–11.
[73] F. Abeles, Optical Properties of Solids, North-Holland Publishing Company, Amsterdam, London, 1972.
[74] E. Kaya, N. Turan, B. Gündüz, N. Çolak, H. Körkoca, Synthesis, characterization of poly-2-(2-hydroxybenzylideneamino)-6-phenyl-4,5,6,7-tetrahydrobenzo[*b*] thiophene-3-carbonitrile: Investigation of antibacterial activity and optical properties, Polym. Eng. Sci. 52 (7) (2012) 1581–1589.
[75] N. Turan, E. Kaya, B. Gündüz, N. Çolak, H. Körkoca, Synthesis, characterization of poly(E)-3-amino-4-((3-bromophenyl)diazenyl)-1H-pyrazol-5-ol: Investigation of antibacterial activity, fluorescence, and optical properties, Fibers Polym. 13 (4) (2012) 415–424.
[76] S. Adachi, Optical Constants of Crystalline and Amorphous Semiconductors, Kluwer Academic Publishers, 1999.
[77] B. Gündüz, M. Cavaş, F. Yakuphanoğlu, Production of Al_2O_3 thin films for FET and MOSFET transistor gate applications, in: 6th International Advanced Technologies, Symposium (IATS'11), 16–18 May 2011, pp. 574–578.
[78] W.G. Spitzer, H.Y. Fan, Determination of optical constants and carrier effective mass of semiconductors, Phys. Rev. 106 (1957) 882–890.
[79] J. Taue, in: F. Abeles (Ed.), Optical Properties of Solids, North-Holland, Amsterdam, 1972.